Title Page:

Cellular and molecular underpinnings of functional networks in the human brain

Guozheng Feng[1], Jiayu Chen[1], Jing Sui[2], Vince D. Calhoun[1*]

[1]Tri-Institutional Center for Translational Research in Neuroimaging and Data Science (TReNDS), Georgia State University, Georgia Institute of Technology, and Emory University, Atlanta, GA, USA;

[2]State Key Laboratory of Cognitive Neuroscience and Learning & IDG/McGovern Institute for Brain Research, Beijing Normal University, Beijing, China.

[*]**Corresponding To:**

Vince D. Calhoun, PhD, Tri-Institutional Center for Translational Research in Neuroimaging and Data Science (TReNDS), Georgia State University, Georgia Institute of Technology, and Emory University, Atlanta, GA, USA; E-mail: vcalhoun@gsu.edu.

Abstract

Understanding how cellular and molecular architecture underpins the large-scale organization of human brain function is a central challenge in neuroscience. By integrating transcriptomic (microarray data and single-nucleus RNA-sequencing [sn-RNA] data), molecular imaging, and neuroimaging datasets, we present converging evidence that the spatial distribution of diverse cell types, neurotransmitter systems, and mitochondrial phenotypes are systematically aligned with intrinsic connectivity networks (ICNs)—the macroscale scaffolding of brain function. These associations extend beyond local correspondence to reflect network-level structure: inter-ICN similarity networks derived from cellular and molecular profiles significantly recapitulate both static and dynamic patterns of functional network connectivity (FNC), mirroring the established division of ICNs into canonical functional domains. Importantly, these cellular and molecular profiles not only co-localize with ICNs and FNC but also appear to support their role as intermediaries linking microscale biological substrates to cognitive function. Mediation analyses reveal that specific ICNs statistically mediate the relationship between microscale cell-type architecture and domain-specific cognitive and behavioral processes. Moreover, dynamic FNC, particularly in specific transient states, captures the mediating pathways linking cell-type and neurotransmitter similarity networks to cognitive network organization. Taken together, our findings suggest that the brain's functional architecture is systematically aligned with cellular and molecular organization, which may act as a biological constraint guiding functional network formation and shaping the neural basis of cognition.

Keywords: cell types, intrinsic connectivity network, functional networks, cognitive function, transcriptomic, cellular and molecular regulation

Introduction

Advances in study of brain networks with resting-state functional MRI (rs-fMRI) have significantly deepened our understanding of both typical and atypical neural activity[1-6]. Among various analytic approaches, decomposition-based independent component analysis (ICA) enables the reliable extraction of intrinsic connectivity networks (ICNs), which reflect coherent patterns of spontaneous brain activity within spatially overlapping but functionally distinct regions[7-9]. These ICNs provide a spatial framework, which can be used to construct inter-network relationships, forming what is known as the functional network connectivity (FNC). The macroscale functional brain networks emerge from the dynamic interplay of distributed neural circuits, whose activity is orchestrated by microscale cellular and molecular processes[10-16]—including cellular composition, neurotransmitter signaling and mitochondrial metabolism. Despite growing evidence for the relevance of these cellular and molecular factors, their specific contributions to the organization of functional network remain largely uncharacterized.

The growing availability of high-resolution cellular and molecular atlases of the human brain—such as microarray-based transcriptional data from the Allen Human Brain Atlas (AHBA)[17], single-nucleus RNA sequencing (snRNA-seq) dataset from discrete brain regions[18-20], and positron emission tomography (PET) imaging of diverse neurotransmitter systems[5]—has created new opportunities to bridge microscale biology with macroscale brain organization. Spatial distributions of specific cell types are increasingly shown to align with the architecture of functional brain networks[21-23]. For example, regional variability in fMRI signals corresponds with the relative abundance of PVALB and SST inhibitory interneurons[21]. Similarly, the brain's principal functional gradient has been linked to spatial patterns of neuronal subtypes—including SNCG and SST interneurons, as well as L5IT and L4IT excitatory neurons[22]. Beyond spatial alignment, molecular similarity further supports the organization of functional networks. Functionally coupled regions often exhibit shared gene expression signatures, suggesting a molecular basis for synchronized activity[24-26]. Concordantly, receptor and transporter similarity across regions correlates with functional connectivity, with brain areas exhibiting similar receptor profiles showing stronger co-activation[27]. In addition, a recent high-resolution atlas of mitochondrial phenotypes offers fresh insights into how energy metabolism contributes to large-scale brain function[19]. Together, these

converging lines of evidence highlight the potential of cellular and molecular atlases to reveal the biological foundations of intrinsic functional networks. Systematic integration of these diverse datasets holds promise for dissecting the spatial and connectional architecture of ICNs, and ultimately, for decoding the molecular logic of large-scale brain dynamics.

The human brain supports a wide range of cognitive and behavioral functions through large-scale neural circuits shaped by its underlying cellular and molecular architecture[15]. At the macroscale, ICNs, as the core organizational units of functional architecture, along with their static and dynamic FNCs, demonstrate heterogeneous contributions to diverse cognitive abilities[28,29]. At the microscale, specific inhibitory neuron subtypes are selectively preserved in individuals who maintain high cognitive performance in late life, implicating cell-type-specific influences on cognitive resilience[30]. Animal studies further underscore the role of molecular processes in cognition and behavior: mitochondrial function has been shown to impact both cognitive capacity[31,32] and behavioral regulation[33,34], while distinct neurotransmitter receptor systems have been associated with specific cognitive domains[35]. The spatial distribution of these receptors differentiates intrinsic and extrinsic cognitive modes[5]. Despite these converging findings, the mechanisms through which ICNs and FNCs mediate the relationship between microscale biological substrates and cognitive and behavior abilities remain poorly understood. Uncovering this linkage is essential for a deeper understanding of how cellular and molecular systems scaffold the brain's functional architecture and enable complex cognition.

In this study, we integrated spatial maps of cell types, neurotransmitter systems, and mitochondrial phenotypes to investigate the cellular and molecular underpinnings of the spatial and connectional architecture of ICNs. We first show that the spatial distribution of these cellular and molecular features is significantly coupled to the spatial organization of the ICNs. We then demonstrate that cellular and molecular architectures constrain inter-network functional connectivity. Finally, we explore the mediating role of ICNs and FNCs in linking microscale biological substrates to spatial and connecitional variations in cognitive and behavioral abilities.

Results

We analyzed 53 reproducible spatial maps of ICNs and their corresponding FNC (Fig. 1A) derived

from the Neuromark_fMRI_1.0 template[7]. The NeuroMark template was based on components which replicated across two large-scale datasets: the Genomics Superstruct Project (GSP; n = 1,005; mean age = 21.54 ± 2.96 years; 411 males)[36] and the Human Connectome Project (HCP; n = 823; mean age = 28.79 ± 3.68 years; 356 males)[37]. To investigate the cellular and molecular architecture underlying ICNs, we systematically examined the spatial and connectional correspondence between these functional networks and a diverse set of cell-type[18], neurotransmitter[27], and mitochondrial[19] maps (Fig. 1B). Extending this analysis, we incorporated 123 cognitive and behavioral probabilistic maps from Neurosynth[38] to assess whether functional networks (ICNs and FNCs) and mediate the relationship between microscale biological substrates and spatial and connectional variations in cognitive and behavioral functions.

Cell-type associates of ICNs. To investigate the cellular architecture underlying ICNs, we related postmortem gene expression–based estimates of cell-type distribution to the spatial maps of 44 cortical ICNs. Bulk tissue transcriptomic data from AHBA[17] were processed using an established harmonization pipeline[39-41]. Cell-type–specific transcriptional signatures were derived from snRNA-seq of eight cortical areas[18], enabling the imputation of 24 cell-type abundances across AHBA samples. These included nine excitatory glutamatergic neurons (e.g., L2/3 IT, L4IT, L6IT), nine inhibitory GABAergic interneurons (e.g., Chandelier, PVALB, SST), and six non-neuronal cell types (e.g., Astro, Endo, Oligo), each characterized by distinct laminar locations, developmental origins, morphology, and projection targets[18,42]. Voxel-level spatial distributions of cell-type abundance were correlated with ICN spatial maps using Spearman's r correlation. Statistical significance was determined using permutation-based two-sided Moran test[43] (1,000 iterations), with false discovery rate (FDR) correction applied across comparisons.

As shown in Fig. 2A, spatial variation in ICNs was significantly associated with the imputed abundance of 17 distinct cell types, spanning 11 ICNs across multiple functional domains. These associations included both positive and negative correlations, indicating that cell-type gradients may support the spatial organization of ICNs. For example, IC6 (superior temporal gyrus network) in the auditory network (AUD) domain showed positive associations with L4IT ($r(146) = 0.50$, $p = 0.02$) and oligodendrocytes ($r(146) = 0.35$, $p < 0.001$), and negative associations with L6IT ($r(146) = -0.25$, $p = 0.02$), L6ITCar3 ($r(146) = -0.25$, $p = 0.04$), L6b ($r(146) = -0.20$, $p = 0.04$), SSTCHODL

(r = -0.45, p = 0.02), and OPC (r(146) = -0.35, p = 0.02). IC10 (paracentral lobule network) and IC14 (precentral gyrus network) in the sensorimotor network (SM) domain were positively associated with endothelial cells (r(82) = 0.47, p < 0.001) and L5ET neurons (r(82) = 0.36, p < 0.001), respectively. IC25 (middle temporal gurus network) in the visual network (VIS) domain correlated with L2/3IT (r(140) = 0.42, p < 0.001), LAMP5LHX6 (r(140) = 0.32, p = 0.03), and VIP (r(140) = 0.25, p = 0.03). IC27 (insula network) in the cognitive-control network (CC) domain was positively associated with L2/3IT (r(127) = 0.43, p = 0.02) and VIP (r(127) = 0.33, p = 0.02), and IC45 in the default mode domain was significantly associated with SSTCHODL (r(139) = 0.44, p = 0.02). A complete summary of cell-type–ICN associations is provided in *Extended Data Table 1*. Spatial distributions of the 17 significantly associated cell types are shown in Fig. 2B, and full spatial distributions for all 24 cell types are presented in *Supplementary Fig. S1*.

Neurotransmitter and mitochondrial associates of ICNs. To examine the neuromodulatory architecture underlying ICNs, we assessed the spatial alignment between ICN maps and neurotransmitter systems using PET-derived estimates of receptor and transporter densities. We compiled 19 neurotransmitter maps encompassing nine neurotransmitter systems, aggregated from PET imaging data across more than 1,200 healthy individuals[27]. These maps included six serotonergic (5-HT_{1A}, 5-HT_{1B}, 5-HT_{2A}, 5-HT_4, 5-HT_6, 5-HTT), three dopaminergic (D_1, D_2, DAT), noradrenergic (NET), histaminergic (H_3), cholinergic ($\alpha_4\beta_2$, M_1, VAChT), cannabinoid (CB_1), opioid (MOR), glutamatergic (NMDA, $mGluR_5$), and GABAergic ($GABA_A$) systems.

For each ICN, we constructed multilinear regression models using the full set of receptor and transporter densities as predictors. Statistical significance was assessed using two-sided Moran test (1,000 permutations) to account for spatial autocorrelation[43], with FDR correction applied across comparisons. Eighteen ICNs exhibited significant model fits (0.43 ≤ adjusted r^2 ≤ 0.86, p < 0.05, Fig. 2A), indicating that distinct combinations of neurotransmitter systems spatially align with ICN architecture. To determine the relative contribution of individual neurotransmitter systems, we applied dominance analysis, which quantifies the proportion of variance in each ICN map attributable to each receptor/transporter in the model[44]. Dominance scores were normalized by the model's total adjusted r^2, enabling comparison across ICNs (Fig. 2B). After controlling for spatial autocorrelation, we found that the NET receptor made a prominent contribution to IC2

(subthalamus/hypothalamus network, contribution = 26%, $p < 0.001$), while DAT significantly contributed to IC3 (putamen network, contribution = 8%, $p = 0.04$). Both D_1 and $\alpha_4\beta_2$ receptors showed significant influence on IC5 (thalamus network, each 33%, $p = 0.02$), highlighting their selective roles in shaping ICNs within the subcortical network (SC) domain. A complete summary of neurotransmitter–ICN associations is provided in *Extended Data Table 2*.

In parallel, we examined the association between mitochondrial phenotypes and ICNs. Six mitochondrial maps (complex I [CI], complex II [CII], complex IV [CIV], mitochondrial density [MitoD], tissue respiratory capacity [TRC], and mitochondria respiratory capacity [MRC])[19] were regressed onto ICN spatial maps. We observed significant model fits for IC2 (adjusted $r^2 = 0.25$, $p < 0.001$) and IC4 (caudate network, adjusted $r^2 = 0.34$, $p < 0.001$), both located in SC domain (*Supplementary Fig. S2*). These findings suggest that mitochondrial energy metabolism may contribute to the functional architecture of specific ICNs in SC domain. A complete summary of neurotransmitter–ICN associations is provided in *Extended Data Table 3*.

Cellular and molecular similarity networks relate to functional connectivity. Having established that ICNs exhibit distinct spatial associations with cellular and molecular features, we next asked whether ICNs that are similarly composed at the cellular and molecular levels also exhibit stronger functional interactions. To this end, we computed similarity networks for cell-type, mitochondrial, neurotransmitter, and combined molecular fingerprints by correlating the mean spatial profiles of each ICN pair using Spearman's correlation (Fig. 3A). Across all modalities, cellular and molecular similarity was significantly greater among ICNs within the same functional domain than between different domains, even after regressing out Euclidean distance and spatial overlap (Dice coefficient) from the similarity matrices ($p < 0.001$, ranksum test; $N_{\text{within}} = 230$ edges, $N_{\text{between}} = 716$ edges for celltype; $N_{\text{within}} = 246$ edges, $N_{\text{between}} = 1{,}132$ edges for others, Fig. 3B). We then assessed the relationship between cellular/molecular similarity and functional connectivity, as indexed by the group-level consensus FNC from the HCP dataset (Fig. 3C). We observed that cell-type similarity (Spearman's r (946) = 0.25, $p < 0.001$), neurotransmitter similarity (Spearman's r (1378) = 0.27, $p < 0.001$), and the combined similarity network (Spearman's r (1378) = 0.46, $p < 0.001$) were all significantly correlated with FNC strength (Fig. 3D). At the regional level, correlations were predominantly positive, with the strongest associations observed in nodes located

within the SM and VIS domains (Fig. 3E, *Extended Data Table 4*). To further investigate the dynamic aspects of this relationship, we identified five discrete states of dynamic FNC (*Supplementary Fig. S3A*) and examined their correspondence with cellular and molecular similarity networks. Results consistently demonstrated robust associations between FNC states and similarity networks, both at the global (*Supplementary Fig. S3B-F*) and regional levels (*Supplementary Fig. S4A-E*). These results suggest that ICNs with similar cellular and molecular compositions are more likely to be functionally coupled, independent of spatial proximity. In particular, ICNs within the same functional domain tend to share cellular and molecular characteristics, supporting the idea that inter-regional communication is constrained by a common microscale architecture. Together, these findings indicate that the cellular and molecular milieu of ICNs contributes to the macroscale organization of functional brain networks.

Identify cellular and molecular structural associations with functional domain. To test whether cellular and molecular profiles reflect the functional domain architecture of ICNs, we constructed similarity networks based on cell-type, mitochondrial, and neurotransmitter fingerprints, while regressing out effects of Euclidean distance and Dice similarity from the network matrices. Using a diffusion embedding method[45], we projected the resulting networks into a common three-dimensional embedding space and applied k-means clustering to identify groups of ICNs with shared cellular and molecular features. The ground-truth labels were derived from the functional domain assignments of ICNs, and clustering performance was quantified using the adjusted Rand index (ARI), with significance assessed via a null generated from 1,000 label permutations. We observed that clustering based on cell-type (ARI = 0.38, $p < 0.001$, 5 clusters; Fig. 4A), mitochondrial (ARI = 0.34, $p < 0.001$, 7 clusters; Fig. 4B), neurotransmitter (ARI = 0.26, $p < 0.001$, 7 clusters; Fig. 4C), and combined profiles (ARI = 0.35, $p < 0.001$, 7 clusters; Fig. 4D) were all significantly aligned with functional domain structures. These findings indicate that the spatial organization of functional domains is underpinned by coherent cellular and molecular architectures.

ICNs mediate the spatial associations between cellular and molecular architecture and cognitive function. To examine whether and how ICNs mediate the relationship between microscale cellular and molecular organization and macroscale cognitive architecture, we leveraged probabilistic meta-analytic activation maps from Neurosynth

(https://github.com/neurosynth/neurosynth)[38]. These maps encode the likelihood that a given cognitive term is associated with activation at each voxel, based on over 15,000 published fMRI studies. A total of 123 cognitive and behavioral terms were selected based on their functional annotations in the Cognitive Atlas[46]. We computed voxelwise correlations between each ICN spatial map and each cognitive probability map. Statistical significance was assessed using two-sided Moran permutation tests (1,000 repetitions)[43], to account for spatial autocorrelation, with multiple comparisons corrected using FDR. We then identified cases where both cellular/molecular maps and cognitive terms were significantly associated with the same ICNs ($p < 0.05$, *Supplementary Fig. S5*). For these shared associations, we conducted mediation analyses using the PROCESS toolbox in R. In each model, the cellular or molecular map served as the predictor, the cognitive probability map as the outcome, and the ICN as the mediator. These analyses reveled 63 significant mediation pathways ($p < 0.05$, Fig. 5, *Extended Data Table 5*), predominantly involving four ICNs, five cell types, and fifty-nine cognitive and behavior functions. These pathways spanned three major domains of cognitive and behavioral function. First, the superior temporal gyrus network (IC6) in the AUD domain mediated the relationship between oligodendrocyte abundance and primary sensory functions, such as perception and listening. This finding aligns with the known role of oligodendrocytes in modulating axonal conduction velocity within auditory pathways[47-49]. Second, the insula network (IC27) in the CC domain mediated associations between L6ITCar3 excitatory neurons and physiological and affective processes, including sleep, balance, and loss. These results suggest a potential contribution of deep-layer excitatory neurons to the functional architecture underlying interoception and emotion-related regulation. Third, the middle frontal gyrus network (IC31) in the CC domain mediated the relationship between Chandelier interneurons and higher-order cognitive functions, such as language, working memory, and cognitive control. This is consistent with the established role of the cognitive control domain in supporting a broad spectrum of behavioral outcomes and higher-order cognition[29,50] and reinforces the view that Chandelier cells shape prefrontal cortical dynamics[51] contributing to neural circuits that support executive functions such as working memory[52]. Overall, our findings highlight specific cell types interface with functional networks to mediate domain-specific cognitive and behavioral phenotypes.

FNC mediate the connectional associations between cellular and molecular architecture

and cognitive function. To further investigate whether inter-ICN functional connectivity (static and dynamic FNCs) mediates the relationship between cellular/molecular similarity and cognitive similarity, we first averaged the cognitive probabilistic maps across the 53 ICNs to obtain ICN-level cognitive features. We then constructed cognitive similarity networks by computing Spearman's correlation between ICNs. Partial Spearman's correlations were performed to assess associations between cellular/molecular similarity networks and the cognitive similarity network, as well as between (static) FNC or dynamic FNC states and the cognitive similarity network. To account for spatial confounds, Euclidean distance and Dice similarity were included as covariates in all correlation and mediation analyses. We found that the cell-type, neurotransmitter, and combined similarity networks were significantly associated with the cognitive similarity network ($p < 0.05$, *Supplementary Fig. S6*). Similarly, both mean (static) FNC and dynamic FNCs from states 1, 2, and 4 showed significant associations with the cognitive similarity network ($p < 0.05$, *Supplementary Fig. S7*). These significant associations were further examined using mediation analyses, where the cellular or molecular similarity network was modeled as the predictor, the cognitive similarity network as the outcome, and the FNC (static or dynamic) as the mediator. The results revealed that dynamic FNC (state 4) partially mediated the relationship between the cell-type similarity network and the cognitive similarity network (path *ab*: $p = 0.05$, $\beta = 0.01$, 95% CI = [0.00, 0.03]; path *c'*: $p = 0.05$, $\beta = 0.08$, 95% CI = [0.00, 0.17]; path *c*: $p = 0.02$, $\beta = 0.10$, 95% CI = [0.01, 0.18], Fig. 7A), and fully mediated the relationship between the neurotransmitter similarity network and the cognitive similarity network (path *ab*: $p = 0.01$, $\beta = 0.04$, 95% CI = [0.01, 0.07]; path *c'*: $p = 0.18$, $\beta = 0.05$, 95% CI = [-0.02, 0.13]; path *c*: $p = 0.01$, $\beta = 0.09$, 95% CI = [0.02, 0.16], Fig. 7B). These results further demonstrate, at the level of network connectivity, that functional networks mediate the foundational influence of cellular and molecular architecture on cognition and behavior. In particular, the mediating role of dynamic FNC (state 4) highlights how transient, state-dependent connectivity patterns can capture biologically meaningful variations that underpin higher-order cognitive processes.

Discussion

By integrating transcriptomic, molecular, and neuroimaging data, we demonstrate that the large-scale functional architecture of the human brain is systematically shaped by its underlying

cellular and molecular organization. Spatial profiles of diverse cell types, neurotransmitter systems, and mitochondrial markers show selective alignment with ICNs, providing a biologically grounded basis for functional segregation. These relationships extend beyond local overlap: similarity networks constructed from molecular and cellular features closely mirror patterns of functional connectivity and recapitulate ICN functional domains. Importantly, ICNs statistically mediate the associations between molecular architecture and cognitive processes, positioning them as critical intermediaries linking microscale biology to behavior. Together, these findings suggest that cellular and molecular organization imposes constraints on the formation and function of large-scale brain networks.

rs-fMRI investigations of intrinsic brain networks have substantially expanded the frontiers of cognitive neuroscience and psychiatric research. Among data-driven approaches, ICA has emerged as a widely used method for decomposing rs-fMRI data into spatially independent functional networks. ICA leverages the hidden spatiotemporal structure of the BOLD signal to separate meaningful neural signals from noise, while preserving subject-level variability[53] and yielding improved signal-to-noise ratios[7]. ICA is a widely used strategy for studying functional networks. It is a data-driven method which leverages higher order statistics to identify the hidden spatial–temporal information to extract spatially independent components while retaining single-subject variability, removing noise components, and enhancing signal-to-noise ratio. Critically, ICA enables the delineation of overlapping but distinct patterns of functional activity, yielding ICN map[54]. Each ICN comprises brain voxels that co-vary over time, capturing intra-network coherence. Functional connectivity between ICNs (FNC) can subsequently be derived by quantifying temporal correlations across their independent time series. To facilitate cross-study reproducibility, methodological advances have led to the fully automated spatially constrained ICA framework (NeuroMark) as template based on 1828 young adult participants (GSP and HCP datasets)[7]. This approach has identified 53 reliable ICNs across large young-adult cohorts (GSP and HCP datasets; N = 1,828), which have since served as functional templates in studies of lifespan development[8], individual differences in cognition[28,55], and a range of neuropsychiatric disorders[56,57]. These large-scale ICNs are thought to arise from the coordinated activity of underlying neural circuits, yet the extent to which they are shaped by microscale cellular and molecular substrates remains poorly understood.

Elucidating the cellular and molecular architecture underlying ICNs and their connectivity patterns (FNC) could offer a foundational neurobiological annotation of functional network organization. Such insights are crucial for bridging levels of analysis from genes and cells to circuits and cognition.

The macroscale functional network organization of the brain is increasingly understood to reflect underlying microscale cellular and molecular architecture[16,21,22]. To explore this hypothesis, we systematically integrated multiple cellular and molecular datasets, including microarray transcriptomic data from AHBA[17], snRNA-seq data[18,19], PET neurotransmitter imaging[27,58]. These data yielded spatial distributions for 24 cell types, 19 distinct neurotransmitter systems, and 6 mitochondrial phenotypes. Mapping these cellular and molecular profiles onto the spatial distribution of ICNs revealed widespread and selective associations. Each ICN exhibited a unique cell-type expression signature, echoing prior findings that functional gradients in cortex are paralleled by distinct cellular composition[22] . Neurotransmitter receptor distributions were broadly predictive of ICN spatial patterns, consistent with the role of neuromodulatory systems in shaping large-scale oscillatory dynamics[59] Notably, mitochondrial phenotypes were preferentially aligned with subcortical ICNs, suggesting a distinct energetic basis for these circuits[10]. Importantly, unlike previous atlas-wide spatial correlation approaches, the ICN-based framework offers a functionally segregated and spatially specific lens for cellular and molecular annotation. ICNs capture voxel-wise coactivation patterns associated with independent functional processes, enabling a finer-grained and functionally dedicated mapping between brain function and neurobiology. This approach advances beyond prior transcriptomic–functional studies by allowing the annotation of individual functional components, rather than broad cortical territories, with targeted cellular and molecular features.

Extending our findings, we observed that ICNs assigned to the same functional domain exhibit significantly greater similarity in their cellular and molecular profiles—across cellular, neurotransmitter, and mitochondrial modalities—compared to ICNs from different domains. These similarities were paralleled by stronger functional co-activation, suggesting that shared microscale composition may facilitate coordinated activity between regions. This supports and expands upon prior work linking transcriptional[24-26,60] and neurotransmitter[29,4] to macroscale brain networks. Clustering similarity networks derived from cellular and molecular fingerprints revealed a non-

random alignment with canonical functional domain assignments. Specifically, ICNs were grouped in a manner that significantly recapitulated known functional subdivisions, suggesting that the brain's cellular and molecular landscape may, in part, mirror the organization of functional networks revealed by group-average fMRI data. These results reinforce the notion that domain-specific functional architectures are underpinned by cell-type and neurotransmitter-specific features. Notably, this molecular-functional alignment echoes anatomical observations from histological analyses, where homogenous cellular composition is observed within local territories, and sharp transitions often demarcate adjacent cortical areas[61]. Interestingly, ICNs within the VIS and SM domains showed higher molecular and functional coupling than those within CC and DM domains, aligning with a previous study of cell-type enriched network structure[22]. This pattern may reflect the preferential enrichment of cell-type and neurotransmitter densities in VIS and SM domains, while CC and DM domains are characterized by smoother transcriptional gradients[62]. These domain-specific molecular architectures may also help explain observed correlation patterns of white matter network[63] and structure–function network coupling[64], highlighting their role in shaping both network identity and inter-network communication.

Cognitive and behavior functions emerge from dynamic neural activity shaped and modulated by underlying cellular and molecular processes[15,64]. Functional network studies have consistently linked specific domains, such as AUD domain with perceptual processing[65] and CC domain with broad behavioral outcomes and higher-order cognition[29,50]. Microscale evidence further implicates distinct cell types in sculpting cognitive capacities[30]. Yet, the extent to which macroscale ICNs and FNCs mediate the relationship between cellular architecture and cognition remains poorly understood. Leveraging a large-scale meta-analytic cognitive atlas, we identified specific ICNs that act as mediators between spatial cell-type distributions and cognitive functions. Notably, the superior temporal gyrus network in the auditory domain mediated the association between oligodendrocyte density and primary perceptual processes such as perception and listening. This is consistent with the role of oligodendrocytes in facilitating rapid saltatory conduction[47] and providing metabolic support[48] for axons, which are critical for auditory information processing[49]. In CC domain, the insular network mediated the relationship between the excitatory L6ITCar3 neurons and affective-behavioral processes. Meanwhile, the middle frontal gyrus network significantly

mediated the link between Chandelier cell distribution and high-level cognitive functions. As potent regulators of pyramidal neuron output, Chandelier cells play a pivotal role in shaping prefrontal cortical activity[51] and are implicated in the neural circuitry supporting working memory[52]. From a network connectivity perspective, we observed significant associations among cellular/molecular similarity networks, static and dynamic FNCs, and the cognitive similarity network. These findings suggest that FNC—particularly its dynamic aspects—may act as a critical bridge linking microscale biological architecture to macroscale cognitive function. The observed mediation effects imply that the alignment between brain biology and behavior is not merely correlative but may be systematically organized through the brain's dynamic communication architecture. In particular, the mediating role of dynamic FNC (state 4) highlights how transient, state-dependent connectivity patterns may encode biologically meaningful variations relevant to higher-order cognition. Together, these findings move beyond simple correlations between cell types and networks or networks and cognition. Instead, they delineate a mediational pathway wherein macroscale functional networks serve as mechanistic conduits linking molecular-scale organization to behavioral phenotypes. This integrative model not only strengthens the biological plausibility of structure–function–cognition relationships but also provides a principled framework for understanding the neurobiological substrates of individual cognitive differences.

While our findings offer novel insights into the cellular and molecular foundations of ICNs, several limitations should be acknowledged. First, the current study focused exclusively on healthy young adults, leaving open the question of whether these molecular–functional associations generalize across developmental stages, aging, or neuropsychiatric conditions. Future work incorporating lifespan and clinical populations will be essential to assess the stability and specificity of these relationships. Second, the cellular and molecular maps used in this study are derived from donor-based atlases, which may obscure individual-level variability due to differences in age, sex, and other demographic factors. As individual-level multi-modal datasets become more widely available, future research could pursue personalized mappings of molecular and functional architecture to better capture inter-individual differences. Third, although we aimed for a whole-brain analysis, our findings are constrained by current data availability in certain regions. In particular, subcortical and cerebellar territories remain underrepresented in many molecular atlases,

and region-specific variability in neurotransmitter receptor expression further limits comprehensive coverage. Expanding spatially resolved molecular datasets—especially in these under-characterized areas—will be vital to building a more complete model of brain-wide molecular–functional coupling.

In summary, this study offers a multi-scale framework linking molecular and cellular architecture to large-scale brain function by integrating transcriptomic and neurotransmitter maps with functional networks. We show that ICNs are not only spatially aligned with, but also structurally constrained by underlying biological features—constraints that extend beyond local correspondence to reflect network-level structure. Moreover, we identify specific ICNs that mediate the translation of molecular substrates into cognitive functions, providing a mechanistic bridge from microscale biology to macroscale behavior. These findings advance our understanding of how functional brain networks emerge from biological structure and lay the groundwork for integrative models spanning molecular neuroscience, functional imaging, and cognition.

Materials and methods

Participants and imaging preprocessing. A total of 823 healthy young adults were selected from HCP (mean age = 28.79 ± 3.68 years; 356 males)[37] (http://www.humanconnectomeproject.org/data) dataset. Comprehensive demographic information and imaging acquisition protocols are described in reference[37]. We used preprocessed rs-fMRI data (http://www.humanconnectomeproject.org/data). The HCP preprocessing pipeline included spatial distortion correction, motion correction, echo planar imaging (EPI) distortion correction, registration to standard Montreal Neurological Institute (MNI) space, and intensity normalization. Subsequently, the data were resampled to 3 × 3 × 3 mm^3 isotropic voxels and spatially smoothed using a Gaussian kernel with a full width at half maximum (FWHM) of 6 mm. The detailed quality control procedure for all the preprocessed data can be found in the reference[7].

ICNs. We utilized 53 ICNs from the Neuromark_fMRI_1.0[7], which has been shown to be meaningful and highly reproducible across independent datasets, including GSP[36] and HCP[37]. Each ICN represents a spatially independent component reflecting coherent brain activity. These ICNs were grouped into seven functional domains based on anatomical and functional priors: subcortical

network (SC, 5 ICNs), auditory network (AUD, 2 ICNs), sensorimotor network (SM, 9 ICNs), visual network (VIS, 9 ICNs), cognitive-control network (CC, 17 ICNs), default-mode network (DM, 7 ICNs), and cerebellar network (CB, 4 ICNs).

FNC. The preprocessed HCP data were decomposed into 53 subject-specific independent components and their associated time courses (TCs) using a spatially constrained single-subject ICA method, with the Neuromark_fMRI_1.0 template serving as spatial priors (available via GIFT at http://trendscenter.org/software/gift)[7]. To minimize residual noise in the ICN TCs, four additional postprocessing steps were applied: (1) detrending to remove linear, quadratic, and cubic trends; (2) outlier detection and removal; (3) multiple regression of six head motion parameters (three translations and three rotations) along with their temporal derivatives; and (4) band-pass filtering (0.01–0.15 Hz). Pearson's correlation were computed between the denoised ICN time courses to generate individual-level FNC matrices, which were then averaged to obtain a group-level FNC matrix. Dynamic FNC was estimated using a sliding-window approach, segmenting the TCs into overlapping temporal windows as described previously[28]. For each segment, we computed covariance from the regularized precision matrix[66] using the graphical LASSO method[67] with an L1 penalty to promote sparsity. The regularization parameter (λ) was optimized for each scan by maximizing the log-likelihood on held-out data[68]. Window-wise FNC estimates were concatenated to yield a subject-level dynamic FNC representation, capturing temporal variations in ICN connectivity. To reduce redundancy, windows were subsampled along the temporal axis. Exemplar windows were selected based on local maxima in FNC variance across connections. These exemplars were clustered using k-means, repeated 500 times with random centroid initializations to ensure stability. The optimal number of states was determined via the elbow criterion[69]. The final centroids were used to assign all windows to discrete states. The fractional rate was quantified as the percentage of windows assigned to each state. For each state, dynamic FNCs were averaged across all windows assigned to that state to generate group-level state-specific FNC patterns.

AHBA microarray data processing. Human brain gene expression data from 3,702 bulk tissue samples across six postmortem brains were obtained from the AHBA dataset (http:// human.brain-map.org/)[17]. Raw data were processed at the sample level using the abagen toolbox (https://abagen.readthedocs.io/en/stable)[39,40], following a standardized and widely recommended

pipeline[39]. Probe reannotation was performed based on data provided in reference[39], and probes lacking Entrez Gene IDs were excluded. To ensure reliability, only probes that exceeded background expression levels in at least 30% of all tissue samples were retained. Among these, the probe with the highest differential stability was selected to represent each gene. After filtering and selection, a total of 16,383 genes were retained. Within each donor, gene expression values were first z-scored across genes within each sample, and then z-scored across all tissue samples.

Cell-type deconvolution. Single-nucleus droplet-based sequencing (snDrop-seq) data[18] were obtained from the cellxgene-census (https://cellxgene.cziscience.com/collections/d17249d2-0e6e-4500-abb8-e6c93fa1ac6f). Gene identifiers were harmonized by matching Entrez Gene IDs between the snDrop-seq and AHBA datasets, retaining only shared genes. To reduce computational load and enhance specificity, we limited the gene set to reliable marker genes consistently identified across eight cortical regions, as reported in reference[18]. Transcriptionally similar cell types were grouped according to the groupings across area subclasses[18,42] to mitigate collinearity in downstream analyses. The aggregated snDrop-seq data across all eight cortical areas were used as a reference to perform cell-type abundance deconvolution of the AHBA bulk tissue samples via BayesPrism[70]. This resulted in estimated abundances for 24 distinct cell types across cortical samples, including: L2/3IT, L4IT, L6IT, L6ITCar3, L5IT, L5ET, L5/6NP, L6CT, L6b, Chandelier, PVALB, SST, SSTCHODL, LAMP5, SNCG, PAX6, LAMP5LHX6, VIP, Astro, Endo, OPC, VLMC, Micro/PVM, and Oligo. For each AHBA donor, estimated cell-type abundances were mapped into MNI space at $3 \times 3 \times 3$ mm³ isotropic resolution using the corresponding MNI coordinates of the tissue samples. Finally, cell-type abundance maps were averaged across all donors to generate group-level spatial distributions for each cell type.

Molecular atlas. We included two sets of molecular maps representing neurotransmitter systems and mitochondrial phenotype. The neurotransmitter receptor and transporter density maps were estimated via 19 PET-derived tracer images from https://github.com/netneurolab/hansen_receptors[27]. The analyzed receptors and transporters included 5-HT_{1A}, 5-HT_{1B}, 5-HT_{2A}, 5-HT_4, 5-HT_6, 5-HTT, D_1, D_2, DAT, NET, H_3, $\alpha_4\beta_2$, M_1, VAChT, CB_1, MOR, NMDA, $mGluR_5$, and $GABA_A$. Six mitochondrial phenotype images were obtained from https://neurovault.org/collections/16418/[19], These phenotypes included CI, CII, CIV, MitoD,

TRC, and MRC. All molecular images were coregistered to MNI space with 3 × 3 × 3 mm^3 isotropic resolution, matching the resolution of the ICN and gene expression data to ensure consistent spatial alignment across modalities.

Cognitive probabilistic measures. We utilized probabilistic maps from Neurosynth (https://github.com/neurosynth/neurosynth)[38] to derive voxel-wise cognitive and behavioral relevance scores. These maps were generated from meta-analyses of over 15,000 published fMRI studies and quantify the probability that a given cognitive term is reported in a study, conditional on the presence of activation at a specific voxel. In total, 123 cognitive and behavioral terms were selected based on the Cognitive Atlas[46]. All cognitive association maps were resampled and aligned to MNI space with 3 × 3 × 3 mm^3 isotropic resolution, consistent with the spatial resolution used for functional, molecular, and gene expression data, ensuring cross-modality comparability.

Linking ICNs with cellular and molecular atlases. To investigate the potential cellular and molecular underpinnings of individual ICNs, we assessed the spatial associations between each ICN map and the cellular and molecular atlases. For each ICN, we applied a threshold of $|z| > 3$ to exclude weakly activated regions and to focus on spatially specific patterns. Only voxels above the threshold were included in the voxelwise spatial correlation analyses. For the cellular atlas, which is limited to cortical regions, we implemented a local neighborhood averaging approach: for each non-zero voxel in the cellular atlas, we extracted ICN values within a 3 mm radius and computed their mean, yielding a matched spatial representation that preserves localization while mitigating noise from sampling sparsity. Accordingly, ICN-to-cell-type associations were computed only within cortical regions. Spatial similarity between ICN maps and cell-type distributions was quantified using Spearman's correlation. For the neurotransmitter and mitochondrial atlases, we employed multivariate linear regression models[27] to estimate the contribution of each molecular map to ICN spatial variance. ICN intensity maps were treated as the outcomes, and the mitochondrial or neurotransmitter profiles were entered as predictors. The adjusted r^2 was used to quantify the model fit. To evaluate the relative importance of each feature, we used the relaimpo R package, which partitions the explained variance across predictors[44]. To account for spatial autocorrelation, we performed 1,000 permutations using the two-sided Moran test[43]. Significance was determined by comparing observed statistics (Spearman's r for cell types; adjusted r^2 for neurotransmitter/

mitochondrial models) to null distributions generated from 10,000 spatially constrained surrogate maps. All p-values were corrected for multiple comparisons using the FDR method.

Associations between FNC and cellular/molecular similarity networks. We averaged cellular and molecular features across the 53 ICNs and constructed similarity networks for cell types, neurotransmitter receptor densities, and mitochondrial phenotypes using Spearman's correlation between ICNs. To assess whether these similarity networks recapitulate functional organization, we performed a rank-sum test comparing within-domain versus between-domain connections. Importantly, to control for spatial autocorrelation, we regressed out both Euclidean distance and Dice similarity between ICN spatial maps from all connectivity matrices. Next, we assessed the global and regional alignment between the FNC and each cellular/molecular similarity network using partial Spearman's correlation, again controlling for spatial proximity (Euclidean distance and Dice similarity).

Structural associations between ICNs and cellular/molecular architecture. To investigate whether the functional domain structure of ICNs is underpinned by cellular and molecular organization, we first constructed cellular and molecular similarity networks while controlling for spatial autocorrelation (Euclidean distance and Dice similarity) across ICNs. We then applied a diffusion embedding method[45] to project these similarity networks into a shared three-dimensional space. Following this, we used k-means clustering to group the projected connections. The number of clusters was determined based on the number of known functional domains: 5 clusters for the cellular atlas and 7 clusters for the neurotransmitter/mitochondrial atlas. The cluster labels derived from this unsupervised embedding were compared to the true functional domain labels of the ICNs. The ARI was used to quantify the accuracy of the clustering, and 1,000 label permutations were performed to assess the statistical significance of the results.

Mediation analysis. To explore how different ICNs mediate the relationship between cellular and molecular spatial maps and cognitive maps, we first calculated the spatial correlations between each ICN and 123 cognitive probabilistic measures using Spearman's correlation. The *p*-values were corrected for spatial autocorrelation through 1,000 repetitions of the two-sided Moran test[43], and FDR was used to adjust for multiple comparisons. Next, for the ICNs that showed significant spatial correlations with both cellular/molecular maps and cognitive probabilistic measures, we conducted

mediation analyses using PROCESS. In these analyses, the cellular/molecular maps served as the predictor, the cognitive probabilistic measures were the outcome, and the ICN acted as the mediator. The significance of the mediation was estimated by a bias-corrected bootstrap approach with 1,000 random samplings. FDR was applied to correct the *p*-values for mediation analysis.

To further investigate whether inter-ICN functional connectivity (FNC and dynamic FNC) mediates the relationship between cellular/molecular similarity and cognitive similarity, we first averaged the cognitive probabilistic maps across the 53 ICNs to obtain ICN-level cognitive features. We then constructed cognitive similarity networks by computing Spearman's correlation between ICNs. Partial Spearman's correlations were performed to assess associations between cellular/molecular similarity networks and the cognitive similarity network, as well as between (static) FNC or dynamic FNC states and the cognitive similarity network. To account for spatial confounds, Euclidean distance and Dice similarity were included as covariates in all correlation and mediation analyses. We analyzed to identify shared network associations with cellular/molecular similarity networks and FNCs. Instances in which both a cellular/molecular similarity network and the cognitive similarity network were significantly associated with the same FNC were subjected to mediation analysis. Mediation analyses were conducted using the PROCESS, with the cellular/molecular similarity network specified as the predictor, the cognitive similarity network as the outcome, and FNC or dynamic FNC as the mediator. The significance of the mediation was estimated by a bias-corrected bootstrap approach with 1,000 random samplings.

Figure Legends

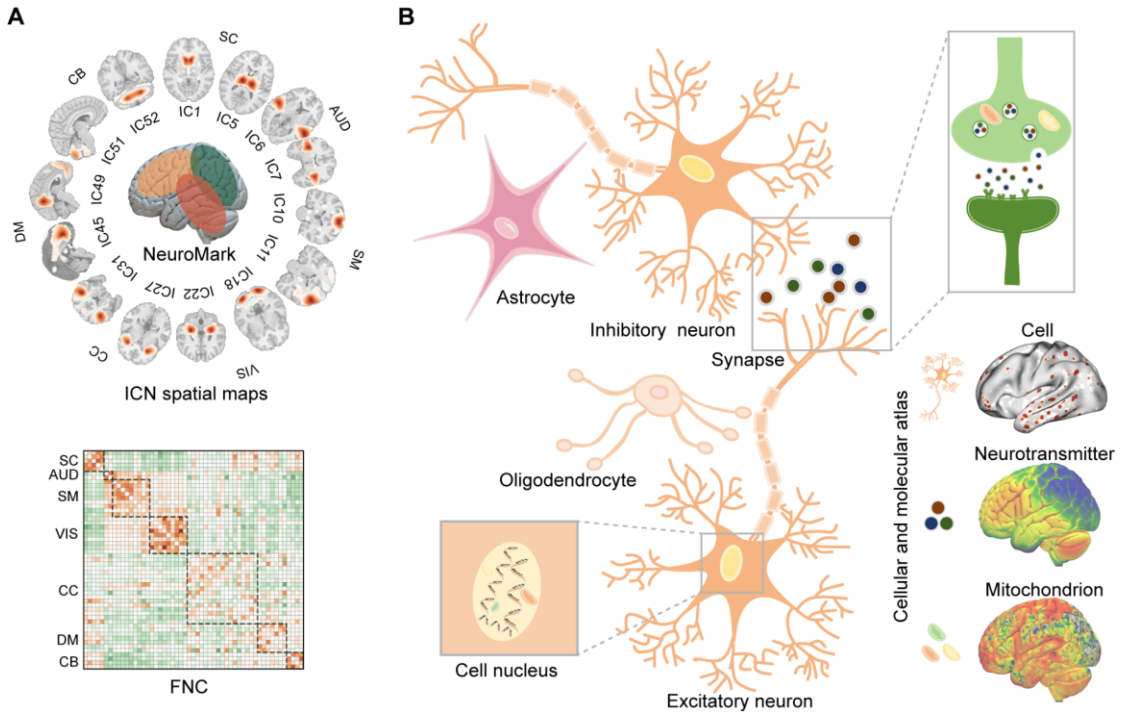

Fig. 1 | ICNs and cellular and molecular process. A. Fifty-three robust and replicable ICNs were identified and organized into seven canonical functional domains using the Neuromark_fMRI_1.0[7], derived from rs-fMRI data of 1,828 young adults across the GSP and HCP cohorts. Each ICN comprises brain voxels that co-vary over time, capturing intra-network coherence. Functional connectivity between ICNs (FNC) captures the inter-ICN coupling by quantifying temporal correlations between their respective time courses. **B.** A diverse set of cellular and molecular maps derived from transcriptomic data (microarray and snRNA-seq) and molecular imaging data (PET), illustrates regional variations in cellular composition, mitochondrial metabolism, and neurotransmitter signaling, providing a multiscale context for interpreting ICN organization.

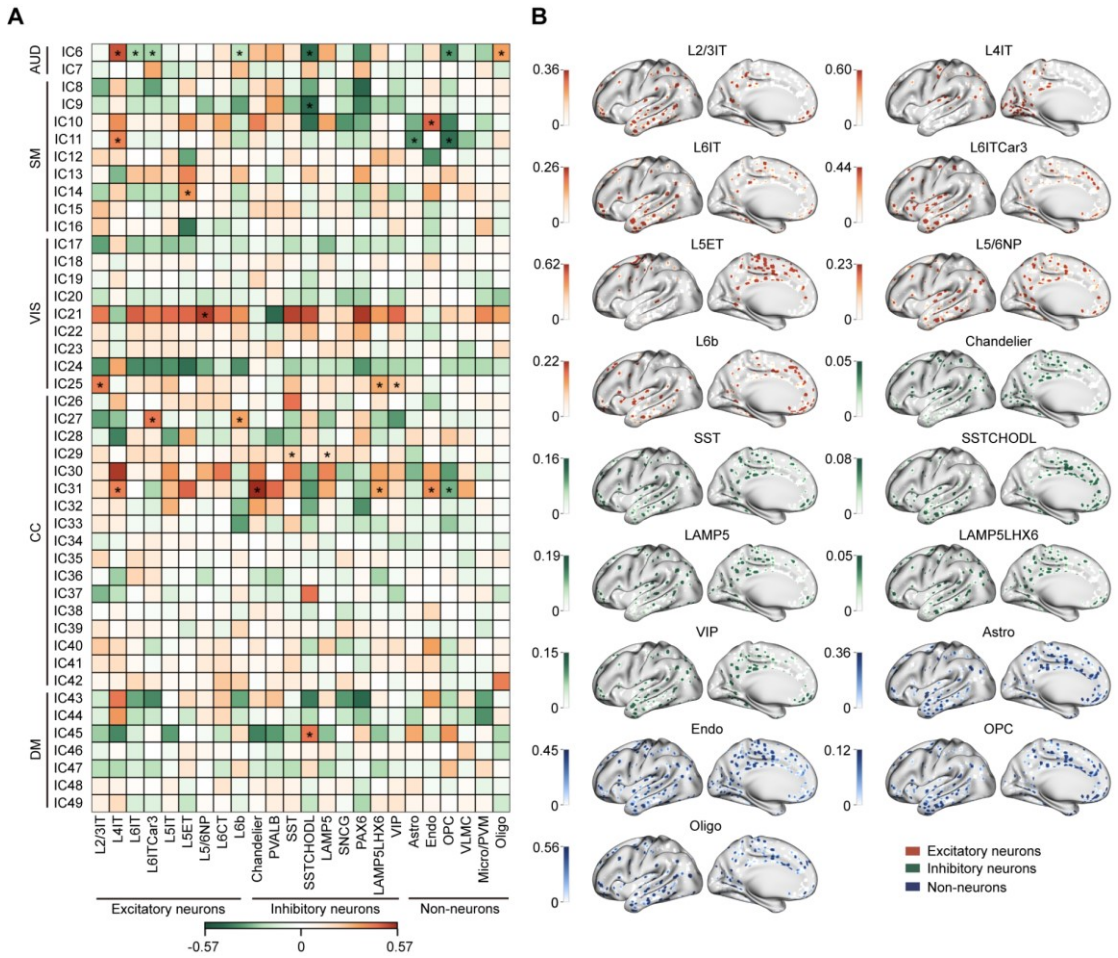

Fig. 2. | Cell-type associates of ICNs. Imputed spatial distributions of 24 cortical cell types were derived by integrating bulk tissue transcriptomic data from the AHBA[17] with snRNA-seq from eight cortical regions[18,42]. Voxel-wise abundance maps were correlated with the spatial patterns of 44 cortical ICNs using Spearman's correlation. Statistical significance was determined using a two-sided Moran test[43] (1,000 iterations), with FDR correction applied across comparisons. **A.** Seventeen cell types showed significant spatial associations with 11 ICNs spanning multiple functional domains, encompassing both positive and negative correlations. These findings suggest that spatial gradients in cellular composition may underpin the large-scale organization of functional brain networks. **B.** Cortical distribution maps of the 17 significantly associated cell types. Note: *: $p < 0.05$.

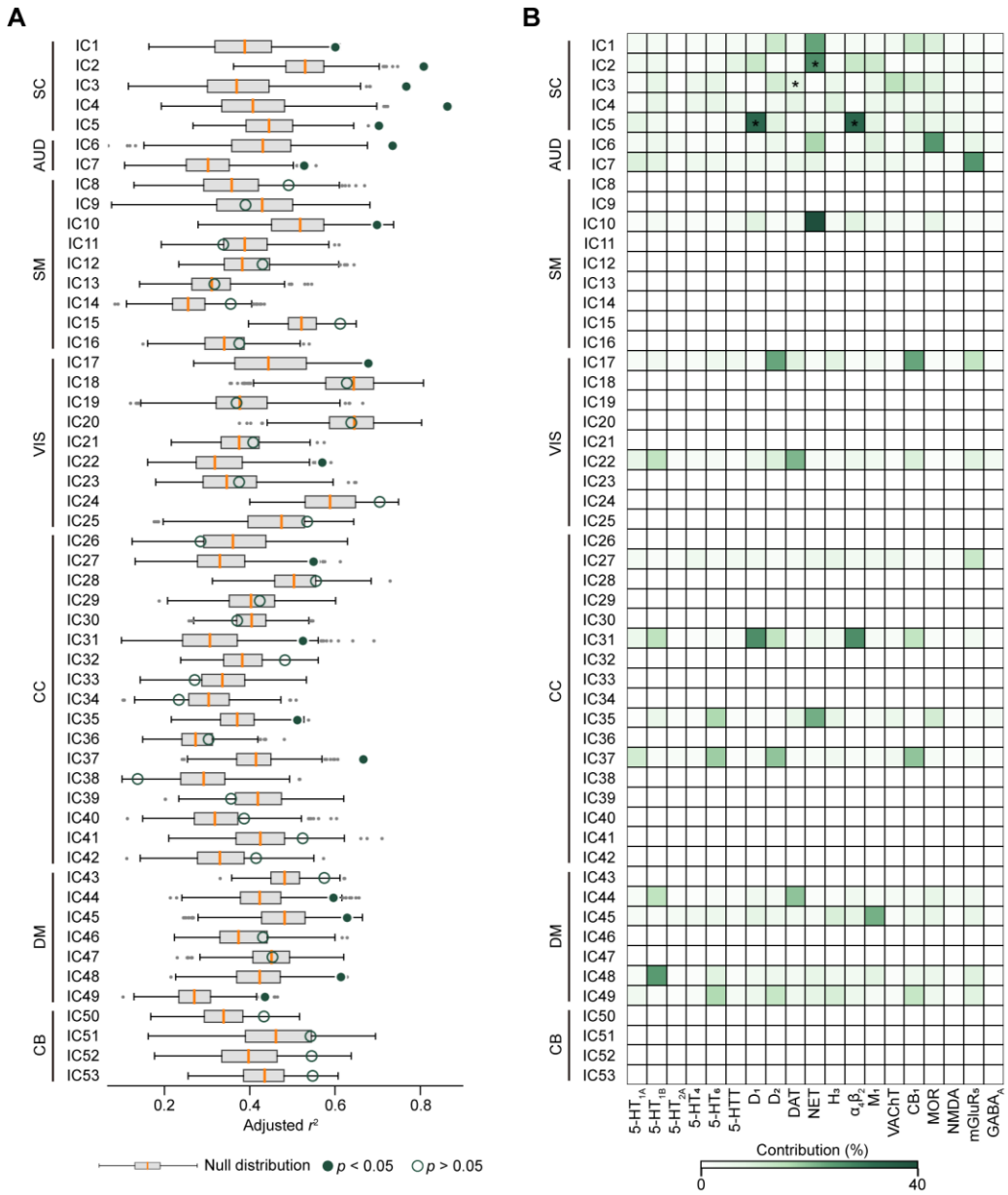

Fig. 3. | Neurotransmitter associates of ICNs. A multilinear regression framework was used to evaluate the spatial correspondence between 53 ICNs and the distribution of 19 neurotransmitter receptors and transporters, as estimated by PET imaging[27]. Dominance analysis was performed to quantify the unique variance in each ICN map attributable to individual receptor/transporter densities[44]. Statistical significance was assessed using Moran test (1,000 permutations) to account for spatial autocorrelation[43], with FDR correction applied across comparisons. **A.** Eighteen ICNs demonstrated significant model fits ($0.43 \leq$ adjusted $r^2 \leq 0.86$), indicating that distinct combinations of neurotransmitter systems spatially align with ICN architecture. Box plots show the median and interquartile range (IQR; 25–75%), with whiskers indicating 1.5× IQR from the first or third quartile.

583 **B.** Dominance analysis revealed that three ICNs within the SC domain were selectively shaped by

584 specific receptor/transporter profiles. Note: *: $p < 0.05$.

585

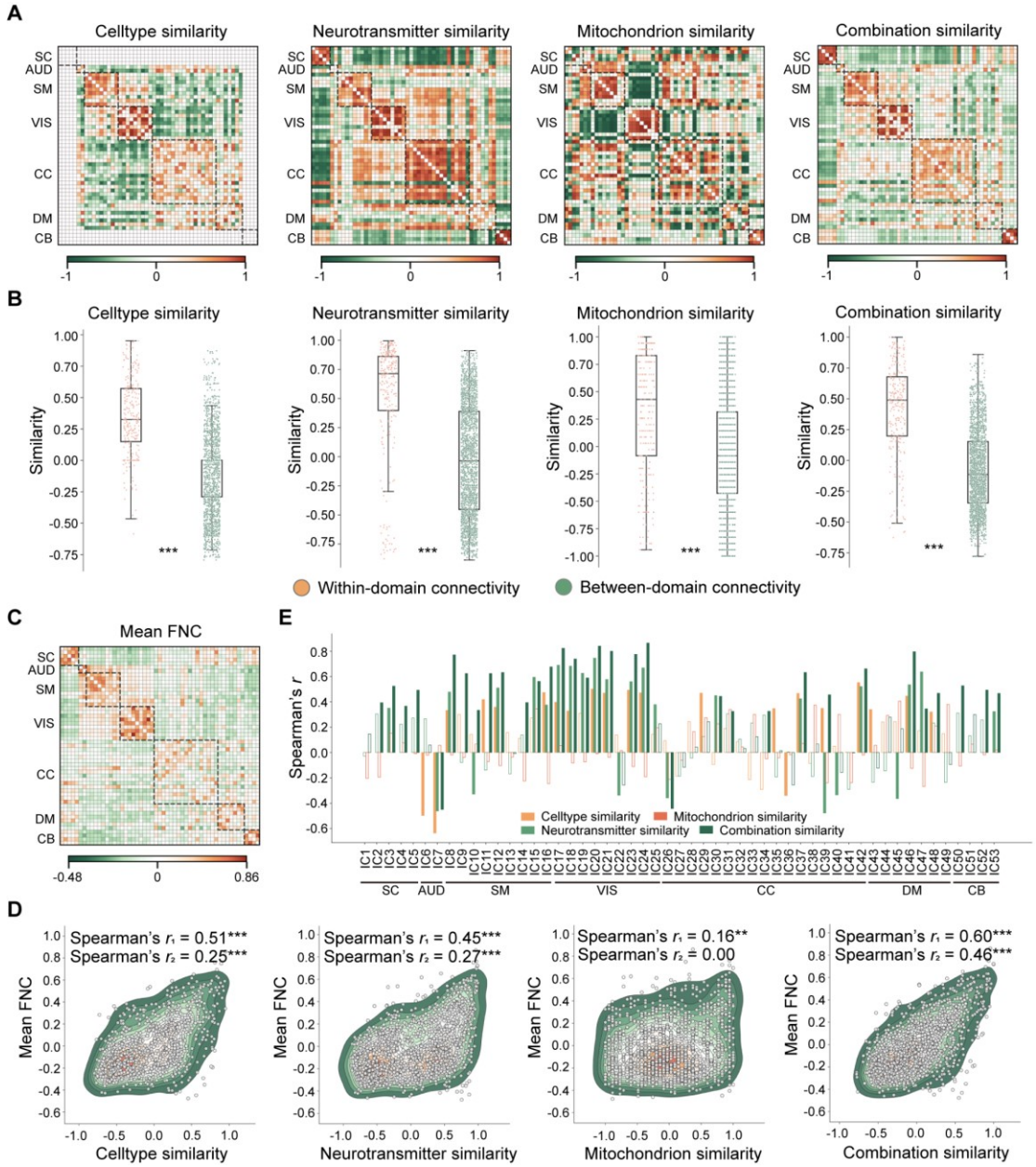

Fig. 4. | Cellular and molecular similarity networks relate to functional connectivity. A. Similarity networks were constructed for cell-type composition, mitochondrial gene expression, neurotransmitter receptor density, and an integrated molecular profile by computing pairwise Spearman correlations between the spatial fingerprints of all ICN pairs. **B.** Within-domain versus between-domain similarity was compared across these networks using a rank-sum test, with confounding effects of spatial proximity (Euclidean distance) and spatial overlap (Dice similarity) regressed out. Box plots show the median and interquartile range (IQR; 25–75%), with whiskers indicating 1.5× IQR from the first or third quartile. **C.** Mean FNC. Global (**D**) and regional (**E**)

associations between FNC and cellular/molecular similarity networks were evaluated using partial Spearman's correlation, controlling for spatial proximity. FDR correction was applied across comparisons. In panel **E**, filled bars indicate statistically significant associations ($p < 0.05$), whereas unfilled bars denote non-significant results. Note: r_1 denotes partial Spearman's correlation without controlling for spatial proximity; r_2: denotes the correlation after controlling for spatial proximity. **: $p < 0.01$; ***: $p < 0.001$.

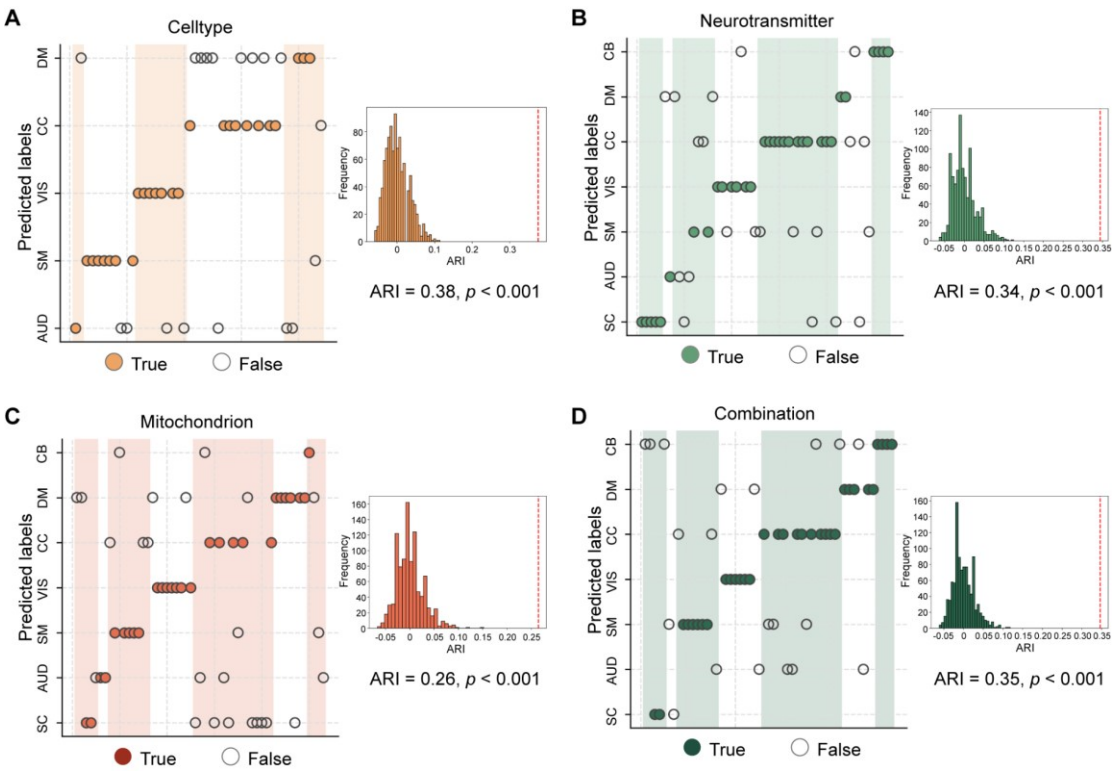

Fig. 5. | Structural associations between ICNs and cellular/molecular architecture. Based on constructed cellular and molecular similarity networks controlling for spatial proximity across ICNs, a diffusion embedding method[45] to project these similarity networks into a shared three-dimensional space. K-means clustering was then performed on the embedded coordinates, with the number of clusters determined by the number of established functional domains: five clusters for the cell-type similarity network (**A**), and seven for the neurotransmitter (**B**), mitochondrial (**C**), and combined (**D**) networks. The cluster labels derived from this unsupervised embedding were compared to the true functional domain labels of the ICNs. The ARI was used to quantify the accuracy of the clustering, and 1,000 label permutations were performed to assess the statistical significance of the results.

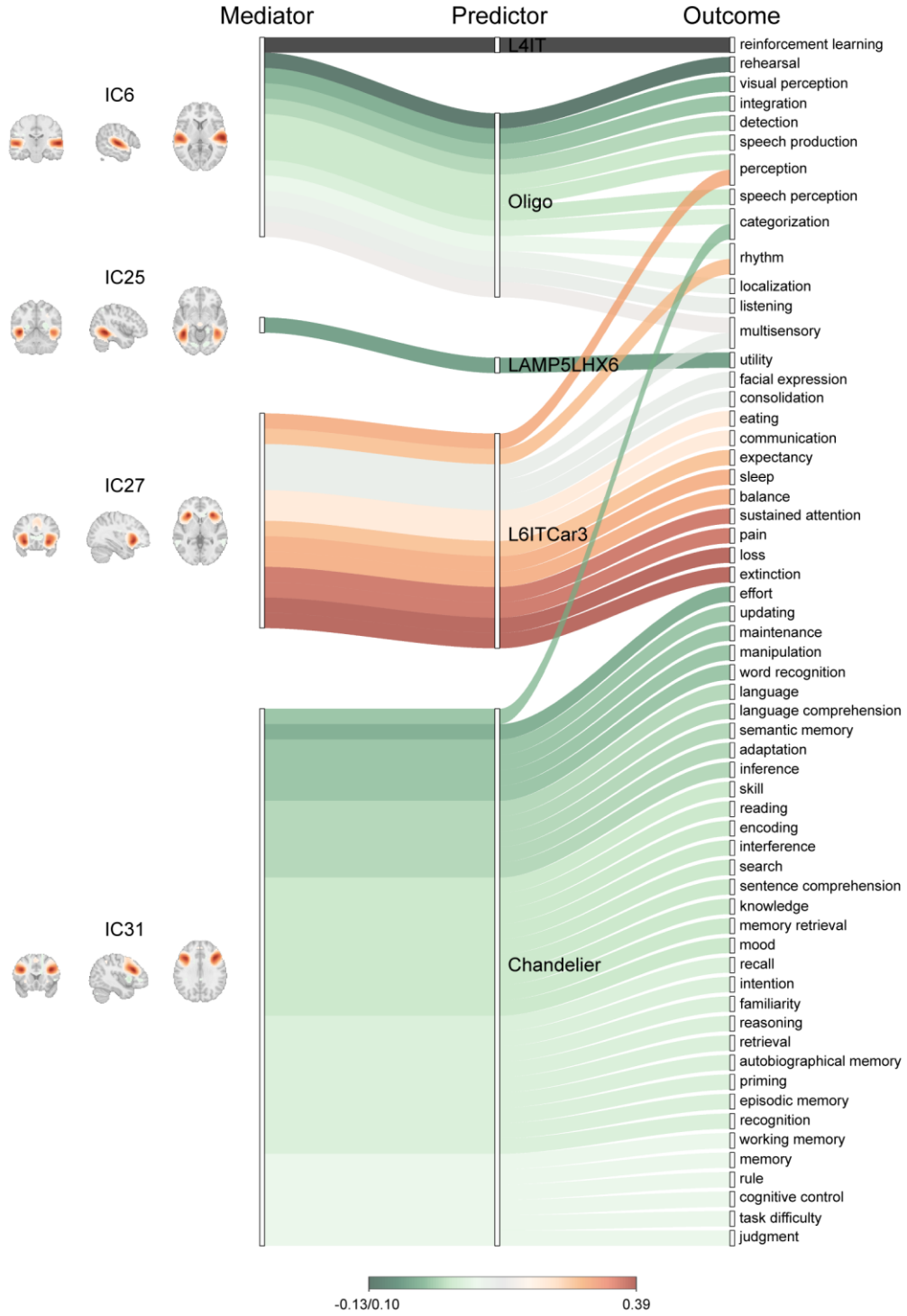

Fig. 6 | ICNs mediate the spatial associations between cellular and molecular architecture and cognitive function. We analyzed 123 probabilistic cognitive activation maps derived from meta-analyses in Neurosynth[38] to identify shared spatial associations with cellular/molecular features and ICNs. Instances in which both a molecular or cellular map and a cognitive term were significantly associated with the same ICN were subjected to mediation analysis. In these models, the molecular or cellular feature served as the predictor, the cognitive activation map as the outcome, and the ICN

621 as the mediator. FDR was applied to correct the *p*-values for mediation effects. Edges in the diagram
622 represent significant mediation pathways, with color indicating the magnitude of the mediation
623 effect.
624

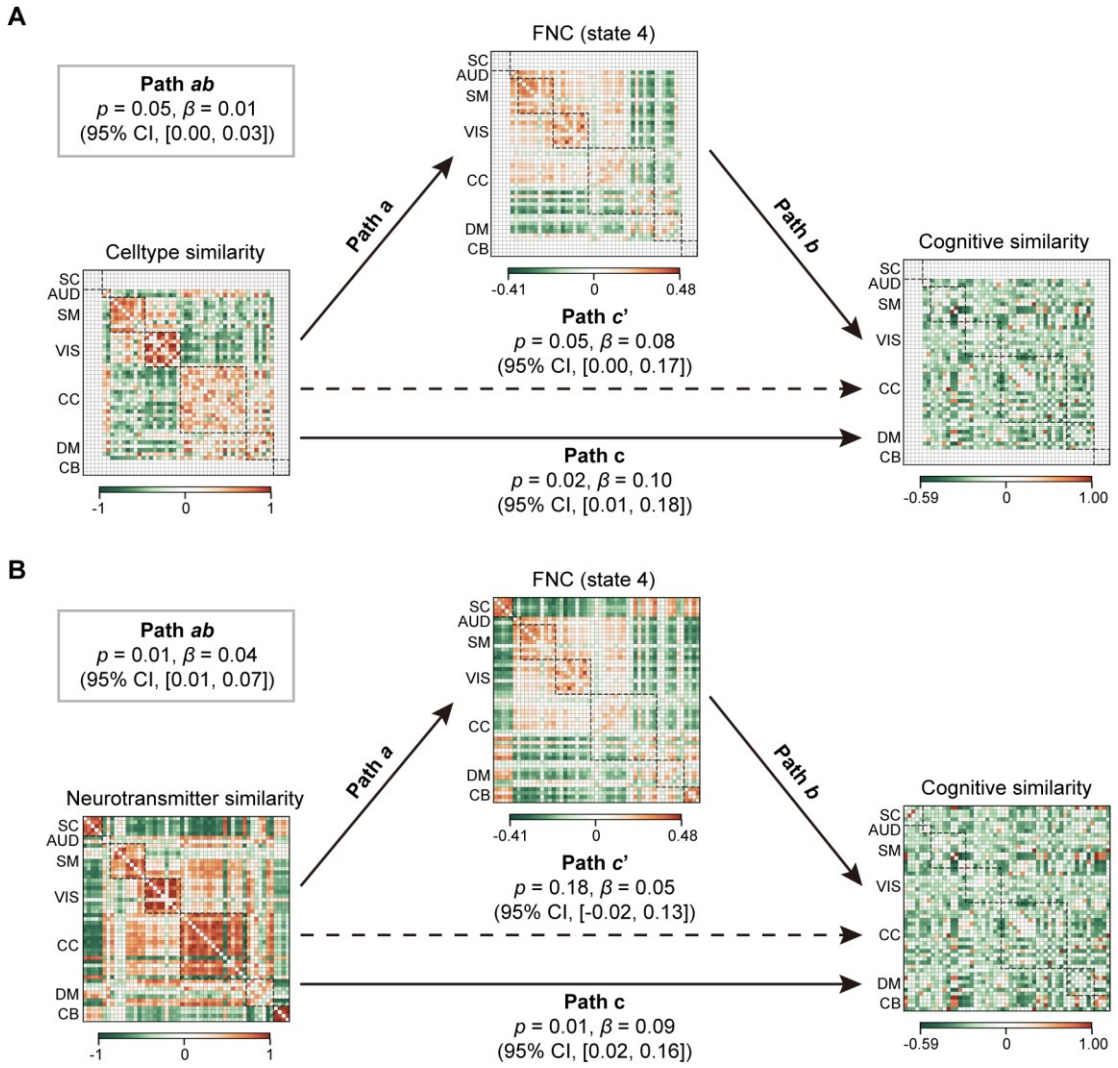

Fig. 7 | FNC mediate the spatial associations between cellular and molecular architecture and cognitive function. Based on 123 probabilistic cognitive activation maps derived from meta-analyses in Neurosynth[38], a cognitive similarity network was constructed by computing pairwise Spearman correlations between the spatial fingerprints of all ICN pairs. We then examined shared network-level associations among cellular/molecular similarity networks, FNCs, and cognitive similarity network. FNCs that were significantly associated with both cellular/molecular and cognitive similarity networks were further tested in mediation models. In these models, the molecular or cellular network served as the predictor, the cognitive similarity network as the outcome, and the FNC as the mediator. **A.** Dynamic FNC (state 4) partially mediated the association between the cell-type similarity network and the cognitive similarity network. **B.** Dynamic FNC (state 4) fully mediated the association between the neurotransmitter similarity network and the cognitive similarity network.

Data and Code availability

The HCP dataset is publicly available at http://www.humanconnectomeproject.org/data. The Neuromark_fMRI_1.0 template is available at http://trendscenter.org/software/gift. The AHBA data can be accessed at http:// human.brain-map.org/ and the sn-RNA dataset is available at https://cellxgene.cziscience.com/collections/d17249d2-0e6e-4500-abb8-e6c93fa1ac6f. Neurotransmitter PET imaging can be found at https://github.com/netneurolab/hansen_receptors and mitochondrial phenotype images can be found at https://neurovault.org/collections/16418/. SPM12 is available at http://www.fil.ion.ucl.ac.uk/spm/ , and the GIFT toolbox can be accessed at http://trendscenter.org/software/gift. The resulting data and code relevant to this study can be accessed through the following links: https://github.com/trendscenter/ICNs-annotation and https://github.com/FelixFengCN/ICNs-annotation. Other codes of this study can be obtained from the corresponding author.

Acknowledgement

The authors thank all the volunteers for their participation in the study and anonymous reviewers for their insightful comments and suggestions. This work was supported by NSF Grant #2112455 and NIH grant #R01MH123610. This work used transcriptomic data from the Allen Institute for Brain Science. Neuroimaging data were provided by the HCP, WU-Minn Consortium (principal investigators: D.V. Essen and K. Ugurbil; 1U54MH091657), funded by the 16 NIH Institutes and Centers that support the NIH Blueprint for Neuroscience Research, and by the McDonnell Center for Systems Neuroscience at Washington University. The content of this manuscript solely reflects the views of the authors and may not reflect the views of the Allen Institute, NIH or the HCP consortium investigators.

Financial Disclosures

There are no conflicts of interest, including any financial, personal, or other relationships with people or organizations, for any of the authors related to the work described in the article.

References

1. Smith, S.M., *et al.* Functional connectomics from resting-state fMRI. *Trends Cogn Sci* **17**, 666-682 (2013).
2. Zuo, X.N., *et al.* Human Connectomics across the Life Span. *Trends Cogn Sci* **21**, 32-45 (2017).
3. Perovnik, M., Rus, T., Schindlbeck, K.A. & Eidelberg, D. Functional brain networks in the evaluation of patients with neurodegenerative disorders. *Nat Rev Neurol* **19**, 73-90 (2023).
4. Fornito, A., Zalesky, A. & Breakspear, M. The connectomics of brain disorders. *Nat Rev Neurosci* **16**, 159-172 (2015).
5. Calhoun, V. Dynamic Interactivity Signatures of Mental Health Risk. *Biological Psychiatry* **97**, S24 (2025).
6. Calhoun, V.D., Miller, R., Pearlson, G. & Adalı, T. The chronnectome: time-varying connectivity networks as the next frontier in fMRI data discovery. *Neuron* **84**, 262-274 (2014).
7. Du, Y., *et al.* NeuroMark: An automated and adaptive ICA based pipeline to identify reproducible fMRI markers of brain disorders. *Neuroimage Clin* **28**, 102375 (2020).
8. Fu, Z., *et al.* Searching Reproducible Brain Features using NeuroMark: Templates for Different Age Populations and Imaging Modalities. *Neuroimage* **292**, 120617 (2024).
9. Iraji, A., *et al.* Identifying canonical and replicable multi-scale intrinsic connectivity networks in 100k+ resting-state fMRI datasets. *Hum Brain Mapp* **44**, 5729-5748 (2023).
10. Shine, J.M. Neuromodulatory Influences on Integration and Segregation in the Brain. *Trends Cogn Sci* **23**, 572-583 (2019).
11. Zhang, D. & Raichle, M.E. Disease and the brain's dark energy. *Nat Rev Neurol* **6**, 15-28 (2010).
12. Cossart, R. & Garel, S. Step by step: cells with multiple functions in cortical circuit assembly. *Nat Rev Neurosci* **23**, 395-410 (2022).
13. Vanderhaeghen, P. & Polleux, F. Developmental mechanisms underlying the evolution of human cortical circuits. *Nat Rev Neurosci* **24**, 213-232 (2023).
14. Paquola, C., Amunts, K., Evans, A., Smallwood, J. & Bernhardt, B. Closing the mechanistic gap: the value of microarchitecture in understanding cognitive networks. *Trends Cogn Sci* **26**, 873-886 (2022).
15. Lee, A.T., Chang, E.F., Paredes, M.F. & Nowakowski, T.J. Large-scale neurophysiology and single-cell profiling in human neuroscience. *Nature* **630**, 587-595 (2024).
16. Bazinet, V., Hansen, J.Y. & Misic, B. Towards a biologically annotated brain connectome. *Nat Rev Neurosci* (2023).
17. Hawrylycz, M.J., *et al.* An anatomically comprehensive atlas of the adult human brain transcriptome. *Nature* **489**, 391-399 (2012).
18. Jorstad, N.L., *et al.* Transcriptomic cytoarchitecture reveals principles of human neocortex organization. *Science* **382**, eadf6812 (2023).
19. Mosharov, E.V., *et al.* A human brain map of mitochondrial respiratory capacity and diversity. *Nature* (2025).
20. Lake, B.B., *et al.* Integrative single-cell analysis of transcriptional and epigenetic states in the human adult brain. *Nature biotechnology* **36**, 70-80 (2018).

21. Anderson, K.M., *et al.* Transcriptional and imaging-genetic association of cortical interneurons, brain function, and schizophrenia risk. *Nat Commun* **11**, 2889 (2020).
22. Zhang, X.H., *et al.* The cell-type underpinnings of the human functional cortical connectome. *Nat Neurosci* **28**, 150-160 (2025).
23. Anderson, K.M., *et al.* Convergent molecular, cellular, and cortical neuroimaging signatures of major depressive disorder. *Proc Natl Acad Sci U S A* **117**, 25138-25149 (2020).
24. Anderson, K.M., *et al.* Gene expression links functional networks across cortex and striatum. *Nat Commun* **9**, 1428 (2018).
25. Richiardi, J., *et al.* BRAIN NETWORKS. Correlated gene expression supports synchronous activity in brain networks. *Science* **348**, 1241-1244 (2015).
26. Krienen, F.M., Yeo, B.T., Ge, T., Buckner, R.L. & Sherwood, C.C. Transcriptional profiles of supragranular-enriched genes associate with corticocortical network architecture in the human brain. *Proc Natl Acad Sci U S A* **113**, E469-478 (2016).
27. Hansen, J.Y., *et al.* Mapping neurotransmitter systems to the structural and functional organization of the human neocortex. *Nat Neurosci* **25**, 1569-1581 (2022).
28. Fu, Z., Sui, J., Iraji, A., Liu, J. & Calhoun, V.D. Cognitive and psychiatric relevance of dynamic functional connectivity states in a large (N > 10,000) children population. *Molecular Psychiatry* **30**, 402-413 (2024).
29. Zhi, D., *et al.* Triple Interactions Between the Environment, Brain, and Behavior in Children: An ABCD Study. *Biol Psychiatry* **95**, 828-838 (2024).
30. Mathys, H., *et al.* Single-cell atlas reveals correlates of high cognitive function, dementia, and resilience to Alzheimer's disease pathology. *Cell* **186**, 4365-4385 e4327 (2023).
31. Hara, Y., *et al.* Presynaptic mitochondrial morphology in monkey prefrontal cortex correlates with working memory and is improved with estrogen treatment. *Proc Natl Acad Sci U S A* **111**, 486-491 (2014).
32. Sharpley, M.S., *et al.* Heteroplasmy of mouse mtDNA is genetically unstable and results in altered behavior and cognition. *Cell* **151**, 333-343 (2012).
33. Hollis, F., *et al.* Mitochondrial function in the brain links anxiety with social subordination. *Proc Natl Acad Sci U S A* **112**, 15486-15491 (2015).
34. Gebara, E., *et al.* Mitofusin-2 in the Nucleus Accumbens Regulates Anxiety and Depression-like Behaviors Through Mitochondrial and Neuronal Actions. *Biol Psychiatry* **89**, 1033-1044 (2021).
35. Noudoost, B. & Moore, T. The role of neuromodulators in selective attention. *Trends Cogn Sci* **15**, 585-591 (2011).
36. Holmes, A.J., *et al.* Brain Genomics Superstruct Project initial data release with structural, functional, and behavioral measures. *Sci Data* **2**, 150031 (2015).
37. Van Essen, D.C., *et al.* The WU-Minn Human Connectome Project: an overview. *Neuroimage* **80**, 62-79 (2013).
38. Yarkoni, T., Poldrack, R.A., Nichols, T.E., Van Essen, D.C. & Wager, T.D. Large-scale automated synthesis of human functional neuroimaging data. *Nat Methods* **8**, 665-670 (2011).
39. Arnatkeviciute, A., Fulcher, B.D. & Fornito, A. A practical guide to linking brain-wide gene expression and neuroimaging data. *Neuroimage* **189**, 353-367 (2019).

40. Markello, R.D., *et al.* Standardizing workflows in imaging transcriptomics with the abagen toolbox. *Elife* **10**(2021).
41. Arnatkeviciute, A., Markello, R.D., Fulcher, B.D., Misic, B. & Fornito, A. Toward Best Practices for Imaging Transcriptomics of the Human Brain. *Biol Psychiatry* **93**, 391-404 (2023).
42. Jorstad, N.L., *et al.* Comparative transcriptomics reveals human-specific cortical features. *Science* **382**, eade9516 (2023).
43. Vos de Wael, R., *et al.* BrainSpace: a toolbox for the analysis of macroscale gradients in neuroimaging and connectomics datasets. *Commun Biol* **3**, 103 (2020).
44. Azen, R. & Budescu, D.V. The dominance analysis approach for comparing predictors in multiple regression. *Psychol Methods* **8**, 129-148 (2003).
45. Margulies, D.S., *et al.* Situating the default-mode network along a principal gradient of macroscale cortical organization. *Proc Natl Acad Sci U S A* **113**, 12574-12579 (2016).
46. Poldrack, R.A., *et al.* The cognitive atlas: toward a knowledge foundation for cognitive neuroscience. *Frontiers in neuroinformatics* **5**, 17 (2011).
47. Cohen, C.C.H., *et al.* Saltatory Conduction along Myelinated Axons Involves a Periaxonal Nanocircuit. *Cell* **180**, 311-322.e315 (2020).
48. Lee, Y., *et al.* Oligodendroglia metabolically support axons and contribute to neurodegeneration. *Nature* **487**, 443-448 (2012).
49. Moore, S., *et al.* A role of oligodendrocytes in information processing. *Nat Commun* **11**, 5497 (2020).
50. Feng, G., *et al.* Methodological evaluation of individual cognitive prediction based on the brain white matter structural connectome. *Hum Brain Mapp* **43**, 3775-3791 (2022).
51. Woo, T.U., Whitehead, R.E., Melchitzky, D.S. & Lewis, D.A. A subclass of prefrontal gamma-aminobutyric acid axon terminals are selectively altered in schizophrenia. *Proc Natl Acad Sci U S A* **95**, 5341-5346 (1998).
52. Volk, D.W. & Lewis, D.A. GABA Targets for the Treatment of Cognitive Dysfunction in Schizophrenia. *Curr Neuropharmacol* **3**, 45-62 (2005).
53. Yu, Q., *et al.* Comparing brain graphs in which nodes are regions of interest or independent components: A simulation study. *J Neurosci Methods* **291**, 61-68 (2017).
54. Xu, J., *et al.* Functional network overlap as revealed by fMRI using sICA and its potential relationships with functional heterogeneity, balanced excitation and inhibition, and sparseness of neuron activity. *PLoS One* **10**, e0117029 (2015).
55. Fu, Z., Liu, J., Salman, M.S., Sui, J. & Calhoun, V.D. Functional connectivity uniqueness and variability? Linkages with cognitive and psychiatric problems in children. *Nature Mental Health* **1**, 956-970 (2023).
56. Yan, W., *et al.* A Brainwide Risk Score for Psychiatric Disorder Evaluated in a Large Adolescent Population Reveals Increased Divergence Among Higher-Risk Groups Relative to Control Participants. *Biol Psychiatry* **95**, 699-708 (2024).
57. Du, Y., *et al.* Evidence of shared and distinct functional and structural brain signatures in schizophrenia and autism spectrum disorder. *Commun Biol* **4**, 1073 (2021).
58. Markello, R.D., *et al.* neuromaps: structural and functional interpretation of brain maps. *Nat Methods* **19**, 1472-1479 (2022).
59. Brookes, M.J., *et al.* Investigating the electrophysiological basis of resting state networks using magnetoencephalography. *Proc Natl Acad Sci U S A* **108**, 16783-16788 (2011).

60. Hawrylycz, M., *et al.* Canonical genetic signatures of the adult human brain. *Nat Neurosci* **18**, 1832-1844 (2015).
61. Brodmann, K. Vergleichende Lokalisationslehre der Grosshirnrinde in ihren Prinzipien dargestellt auf Grund des Zellenbaues. (Barth, 1909).
62. Wagstyl, K., *et al.* Transcriptional cartography integrates multiscale biology of the human cortex. *Elife* **12**(2024).
63. Feng, G., *et al.* Longitudinal development of the human white matter structural connectome and its association with brain transcriptomic and cellular architecture. *Communications Biology* **6**(2023).
64. Feng, G., *et al.* Spatial and temporal pattern of structure–function coupling of human brain connectome with development. *eLife* **13**(2024).
65. Wolff, A., *et al.* Intrinsic neural timescales: temporal integration and segregation. *Trends Cogn Sci* **26**, 159-173 (2022).
66. Smith, S.M., *et al.* Network modelling methods for FMRI. *Neuroimage* **54**, 875-891 (2011).
67. Friedman, J., Hastie, T. & Tibshirani, R. Sparse inverse covariance estimation with the graphical lasso. *Biostatistics* **9**, 432-441 (2008).
68. Allen, E.A., *et al.* Tracking whole-brain connectivity dynamics in the resting state. *Cereb Cortex* **24**, 663-676 (2014).
69. Fu, Z., *et al.* Characterizing dynamic amplitude of low-frequency fluctuation and its relationship with dynamic functional connectivity: An application to schizophrenia. *Neuroimage* **180**, 619-631 (2018).
70. Chu, T., Wang, Z., Pe'er, D. & Danko, C.G. Cell type and gene expression deconvolution with BayesPrism enables Bayesian integrative analysis across bulk and single-cell RNA sequencing in oncology. *Nat Cancer* **3**, 505-517 (2022).